Article

Journal of
Nanoscience and Nanotechnology
Vol. 15, 1–10, 2016
www.aspbs.com/jnn

Laser Assisted Synthesis, Structural and Magnetic Characterization of Gadolinium Germano-Silicide Nanoparticles in Liquid

Natalie Tarasenka[1,2], Vladimir Pankov[2], Andrei Butsen[1], and Nikolai Tarasenko[1,*]

[1] *Institute of Physics, National Academy of Sciences of Belarus, 220072, Minsk, Belarus*
[2] *Belarusian State University, Chemical Department, 220006, Minsk, Belarus*

In this paper the ternary $Gd_5(Si_{1-x}Ge_x)_4$ nanoparticles (NPs) were synthesized by laser assisted techniques in liquid and their crystal structure, morphology and magnetic properties were investigated. To prepare compound gadolinium germano–silicide NPs we used laser irradiation processes in two different ways. First, the compound NPs were synthesized by four step process which involved the sequential ablation of silicon, gadolinium and germanium targets followed by additional laser irradiation of the formed colloid. Second, laser irradiation of the relevant target consisted of $Gd_5(Si_{1-x}Ge_x)_4$ alloy produced by thermal melting of the stoichiometric mixture of the virgin components (powders) in an argon atmosphere in a water-cooled graphite oven was used. The last two-step approach was shown to be more effective the production of Gd–Si–Ge alloys for practical applications.

Keywords: $Gd_5Si_2Ge_2$ Alloys, Nanoparticles, Laser Ablation Synthesis, Magnetic Properties.

1. INTRODUCTION

Last decades pulsed laser ablation in liquid media (PLAL) has proved to be an efficient tool for production of NPs with different morphology, composition and structure. It has been shown that varying the composition of the target and surrounding liquid it is possible to produce metallic, semiconductor, oxide and carbide NPs. Depending on the irradiation conditions like the duration of laser pulse, the laser fluence and wavelength, it is possible to fabricate alloyed and core–shell nanostructures, as well as compound NPs.[1–7]

PLAL has an advantage of preparing NPs under ambient conditions and provides the possibility of combination of particle synthesis with functionalization and stabilization of products. These benefits make laser ablation technique especially suitable for production of NPs with the view of their biomedical applications as they require particles to be biocompatible, nontoxic, tunable in size, suitable for efficient clearance from the body and to be stable in water and in physiological solutions.[8–11]

In our previous works using the ablation of the combined target we were able to produce the compound Gd_5Si_4 NPs which can be used in magnetic hyperthermia treatment of tumors.[12,13] Magnetic hyperthermia is a promising form of cancer therapy that employs heating of tumor cells using a.c. magnetic fields.[14–19] During the treatment, cells undergo heat stress in the temperature range of 41–47 °C resulting in activation and initiation of many intra and extracellular degradation mechanisms like protein denaturation, protein folding, aggregation and DNA cross linking that causes inhibition of many cellular functions.[14] The tissue level effects include pH changes, perfusion and oxygenation of tumor micro environment.

The heat mediators in the magnetic hyperthermia treatment can be embodied as implants (thermoseeds) or nanoparticles. In the later case hyperthermia treatment becomes noninvasive. When fluids containing submicron sized magnetic particles are injected, these particles are easily incorporated into the cells and heat up the tumor cells by coupling with the externally applied magnetic field. As a result the whole tumor can be heated up uniformly. For hyperthermia treatment, particles with sizes around the monodomain–multidomain transition, i.e., particles below 50 nm in diameter, are preferred instead the micron-sized (multidomain) particles because of the higher heating efficiency at tolerable magnetic fields (the higher

*Author to whom correspondence should be addressed.

specific absorption rate).[20] In addition some advantages of using NPs are expected because of the higher effective surface areas (easier attachment of ligands), lower sedimentation rates (higher stability) and improved tissular movement.

The efficiency of hyperthermia treatment strongly depends on the temperatures generated at the targeted sites of action, duration of exposure and characteristics of particular cancer cells.[14] Therefore, the main technical problem in realization of magnetic hyperthermia therapy includes control of the tissue temperature and reaching homogeneous temperature distributions. It is known that normal cells are undamaged by treatment for 1 hour at the temperature of up to 44 °C,[21] while the tumor cells are more sensitive to temperature increasing than healthy ones.[15] Therefore one way of solving the problem of overheating is to synthesize biocompatible superparamagnetic NPs with Curie temperature in the range 41–47 °C that can act as temperature control switches in the required temperature range, preventing overheating.[22] In this case, once the particle temperature reaches the Curie temperature the particles will stop responding to the applied field, hence the heating will be maintained at the Curie temperature. Gd-based NPs can be the good candidates for self-controlled hyperthermia treatment due to the largest magnetocaloric effect known near the room temperature, high value of magnetization, environmental stability and vicinity of their magnetic ordering temperature to the required temperature range that allows self-regulated temperature control in a magnetic field.[23–26]

Since gadolinium molecular complexes cause no significant cytotoxic effect they are widely used in such kinds of diagnostics of diseases like magnetic resonance imaging[27–30] and angiography[31] and as therapeutic agents in drug delivery.[32–35] To increase biocompatibility and reduce the toxicity of compound Gd-based NPs they should be covered by stabilizer layer or encapsulated by polymer or organic molecules.

The magnetic ordering temperature of Gd_5Si_4 is 340 K that is higher than the required temperature range (315–320 K).[36] For comparison, magnetic Fe_3O_4 NPs, used in hyperthermia treatment nowadays, have a Curie temperature of $T_C = 585$ °C that is too high for autoregulation of temperature in the desirable range.[37] It is noteworthy that the Curie temperature of Gd_5Si_4 compound NPs can be tuned by partial substituting Si by Ge atoms or Gd by rare earth metals like Ce, Nd, Er, etc.[18, 36]

Therefore the purpose of the present paper was to prepare ternary gadolinium germano–silicide NPs by laser assisted techniques. To obtain $Gd_5(Si_{1-x}Ge_x)_4$ NPs we used laser irradiation processes in two different ways. First, the compound NPs were synthesized by four step process which involved a sequential ablation of silicon, gadolinium and germanium targets followed by the additional laser irradiation of the formed colloid. Second, laser irradiation of the relevant target consisted of $Gd_5(Si_{1-x}Ge_x)_4$ alloy produced by thermal melting of stoichiometric mixture of the virgin components (powders) in the argon atmosphere in a water-cooled graphite oven was used. The magnetic properties of the synthesized compound NPs were studied to determine their capabilities for further medical applications.

2. EXPERIMENTAL DETAILS

The laser ablation experiments were carried out by focusing the radiation of the Nd:YAG laser (LOTIS TII, LS2134D), operating in a double-pulse mode at 1064 nm (energy 80 mJ/pulse, repetition rate 10 Hz, pulse duration 8 ns), on the surface of a target placed in the cell filled with ethanol. In the double-pulse mode a repetitive consequence of two delayed laser pulses is used for ablation. In the double-pulse configuration, the production rate of NPs has been shown to be greater than the sum of the single-pulse production rates.[38] In addition, definite size reduction of the particles in ablation plume can be achieved under conditions of a suitable temporal delays between two laser pulses in result of heating and fragmentation of the ablated material produced by the first laser pulse. The optimal interpulse delay of 10 μs for the double-pulse laser, as it was found previously,[38] was used in our ablation experiments.

Schematic diagram of the laser ablation experiment is presented in Figure 1. The laser fluence at the target surface was about 250 J/cm^2.

To tune the stoichiometry of the final particles the ablation times of each element were chosen as 15, 15 and 40 min for Si, Ge and Gd targets, respectively. This relation was evaluated from the results of the EDX analysis of the ablated product for obtaining the quantities of the ablated Si, Ge and Gd atoms in the solution close to the stoichiometric ones.

Two orders of the sequential ablation of the indicated targets were selected for our experiments:

1. Si–Gd–Ge (Sample A), and
2. Si–Ge–Gd (Sample B).

The formed colloids were additionally irradiated with the unfocused laser beam of the second harmonic

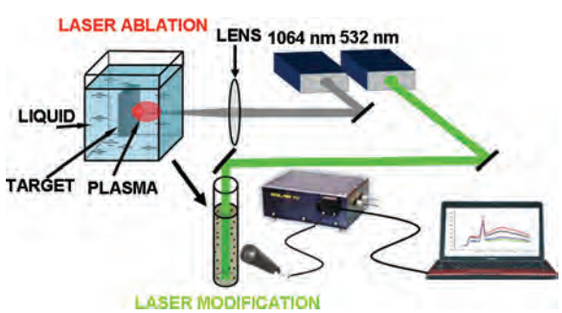

Figure 1. Schematic diagram of the laser ablation experiment with post-ablation irradiation of the formed colloidal solution.

($\lambda = 532$ nm) of the Nd:YAG laser (pulse duration 10 ns, repetition rate 10 Hz) with fluences of 230 and 400 mJ/cm^2.

To implement the method of thermal melting of the stoichiometric mixture of the starting Gd, Si and Ge powders we used a tubular graphite furnace heated by electric current. The basic element of its construction is the tube made of dense graphite. The heating process takes place in the atmosphere of inert gas argon, which protects the graphite furnace from burning.

The graphite furnace was heated in two stages. At the first stage (approximately 10 s), argon was supplied into the furnace without heating in order to displace air from the furnace interior. Then, furnace was quickly heated to the required temperature, controlled in the range of 1000–3000 °C, also with argon in the graphite furnace. The required temperature could be sustained during a certain time interval (2000 °C, 10 s in our experiments), after which the furnace was switched off, and its temperature dropped quickly to the room temperature. The formed alloy sample was re-dispersed in ethanol. The obtained suspension was subjected to the 532 nm laser irradiation to reduce a particles size (Sample C).

Finally, the particles prepared by different ways were characterized by optical emission spectroscopy (OES), transmission (TEM) and scanning (SEM) electron microscopies, X-ray (XRD) and selected area electron diffraction (SAED) analysis as well as by magnetic measurements.

The optical extinction spectra of the colloids were measured by UV-visible spectrophotometer (CARY500). A 1-cm-pathlength-quartz cell was used for these measurements.

TEM was used for studying the size distributions of the resulting NPs. The average diameters of the particles were estimated from the TEM micrographs which were obtained on a LEO 906E (LEO, UK, Germany) transmission electron microscope operated at 120 keV. Samples for TEM were deposited on the copper grids covered by Formvar films. Normally, up to 100 particles are counted to determine the size distribution of each sample. Using this equipment it was possible to study the phase composition of the produced NPs by SAED. The camera constant λL in our experiments was 1.591, camera length—50 cm.

To determine the chemical composition of the produced NPs a drop of colloidal solution was transferred to a single-crystal silicon substrate and dried at room temperature. The composition of the sample deposited on the substrate was detected using energy dispersive X-ray (EDX) spectrometer attached to the scanning electron microscope (SUPRA 55WDS, Carl Zeiss, Germany).

The powder formed after the drying of colloidal solutions was examined using the X-ray diffractometer D8-Advance (Bruker, Germany). Powder phase composition, its crystalline structure, lattice parameters and grain size were determined using Cu Kα radiation (0.154 nm). The X-ray diffraction measurements were performed in point-by-point mode at 300 K with the following parameters: the collection time at the point 3 s, the angle scanning increment 0.03°. In order to obtain the more precise profile of reflexes the mode with 5 s and 0.010° was used.

The magnetic properties of the nanocomposite particles were analyzed with a vibrating sample magnetometer (Cryogenic, England). The magnetization values were measured as a function of temperature in the range of 77–1000 K in a continuous mode without resetting the sample using a temperature cryostat at the constant magnetic field of 1 kOe. In these experiments the definite amount of the investigated powder (0.0079 g) was placed in a quartz ampoule and evacuated to the pressure $p = 10^{-2}$–10^{-3} Pa. The isothermal field dependences of specific magnetization were measured by the vibrating method at 7, 77 and 300 K at the magnetic fields varied in the range -14 T to $+14$ T.

3. RESULTS

3.1. Properties of NPs Formed by Si–Gd–Ge Sequential Laser Ablation (Sample A)

Figure 2 shows the typical extinction spectra of samples of the suspended NPs prepared by sequential laser ablation of silicon, gadolinium and germanium targets in ethanol: as-prepared (1) and after additional laser irradiation (2). The spectra were corrected to the contribution of the solvent.

As can be seen from Figure 2 the extinction spectra of the colloids are rather featureless and exhibit the gradual decrease in overall absorption with increasing wavelength.

The optical properties of the colloid were found to be susceptible to the additional laser irradiation. As can be seen from the extinction spectrum, the irradiated colloid becomes more transparent in visible spectral region after irradiation. The observed modification of the extinction spectrum can be indicative of the changes not only in

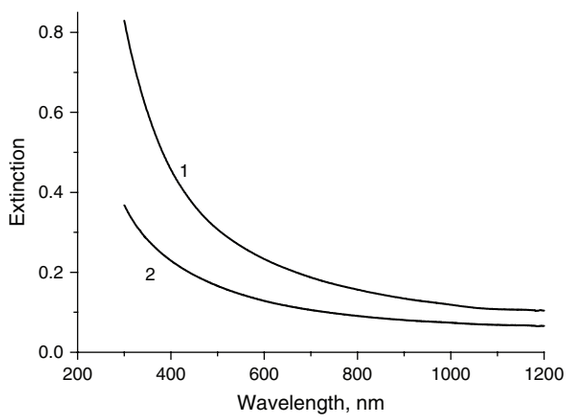

Figure 2. Optical extinction spectra of colloidal solutions produced by sequential laser ablation of silicon, gadolinium and germanium targets as-prepared (1) and after additional laser irradiation (2).

morphology, but also in a composition and structure of the particles subjected to laser irradiation. In particular, decreasing of the extinction in result of post-ablation irradiation can be consistent with the laser-induced fragmentation of larger particles in solutions and as a consequence the lower contribution of scattering to the extinction signal or might be related to the disappearance of the defected structures during the laser treatment process.

The particle morphology was studied using SEM and TEM techniques. The SEM-images of the formed powders are presented in Figure 3. The synthesized powders can be considered as agglomerates (clusters) with sizes in the range 0.5–1.5 μm and each cluster may comprise nanocrystallite. As can be seen from the SEM image 3b, additional laser irradiation of the samples results in the increase of the grain size.

The energy dispersive X-ray (EDX) analysis of both as-prepared and irradiated samples showed the presence only of gadolinium, silicon and germanium in the nanoparticles. Based on the results of the EDX analysis of the ablated products the ratio of atomic content Gd:Si:Ge was adjusted to be close to the stoichiometric one of the $Gd_5Si_2Ge_2$ compound by variation of the duration of ablation of each element.

Details of the morphologic structure of NPs prepared by sequential laser ablation of Si, Gd and Ge targets in ethanol are presented in Figure 4. The microphotographs in Figures 4(a) and (b), that show the TEM images of the particles prepared by laser ablation (1064 nm) of Si target in ethanol and of Gd target in the Si colloidal solution, respectively, reveal that as-prepared colloids consist of two types of particles: small dark spherical particles and larger agglomerates of size more than 60 nm. Most of the dark particles are about 5 nm in diameter with a narrow size distribution. After ablation of Gd in Si colloidal solution the consolidation of small particles into the aggregates is observed, while the size of large particles remains practically unchanged.

The picture becomes more complex after the third step of the process. After the laser ablation of germanium in the colloidal solution produced by sequential ablation of Si and Gd targets in ethanol, the TEM micrograph presented in Figure 4(c) reveals loosely aggregated clusters containing large ($d > 40$ nm) single spherical particles surrounded by a cloud of dust presumably of the amorphous structure.

Laser irradiation by the 532 nm laser beam resulted in the improving of crystallinity of the prepared Si–Gd–Ge particles (Fig. 4(d)). Hereby, the size of the large particles varies slightly.

In order to determine the crystalline structure and phase composition of the prepared nanopowders their X-ray diffraction (XRD) patterns were analyzed. XRD analysis indicated that the synthesized powders exhibited complex phase composition. Two intense broad diffuse bands (halo) in the region of 25–50° can be seen in the X-ray diffraction pattern of as-prepared powder (Fig. 5(a)). Such X-ray patterns are characteristic for the nanopowders consisting of very fine grains, which crystalline structure is significantly distorted or is in a state close to amorphous one.[39–41]

However, the prepared powders are not totally amorphous and some peaks corresponding to the unreacted phases of the initial components: Gd (cubic), Si (cubic), Ge (cubic), as well as a small admixture of graphite, can also be distinguished against the diffuse bands in the presented XRD pattern. The formation of graphite can be explained by the partial decomposition of ethanol during the laser ablation process.[42]

It should be noted that the most intense peaks corresponding to the phases of binary and ternary Gd based compounds are in the region of the diffuse bands, so these phases can present in the colloidal solution, however their identification is hardly possible by XRD method as NPs of the compounds are rather small and have, most likely, the distorted lattice.

The alloys of $Gd_5(Si_{1-x}Ge_x)_4$ series have different crystal structures depending on Si:Ge ratio. They crystallize in orthorhombic structure (so-called orthorhombic I crystal structure) for $0 \leq x < 0.5$ (the Si-rich Gd_5Si_4-type solid solution), whereas the crystal structure changes from orthorhombic to monoclinic for $x \geq 0.5$. The intermediate

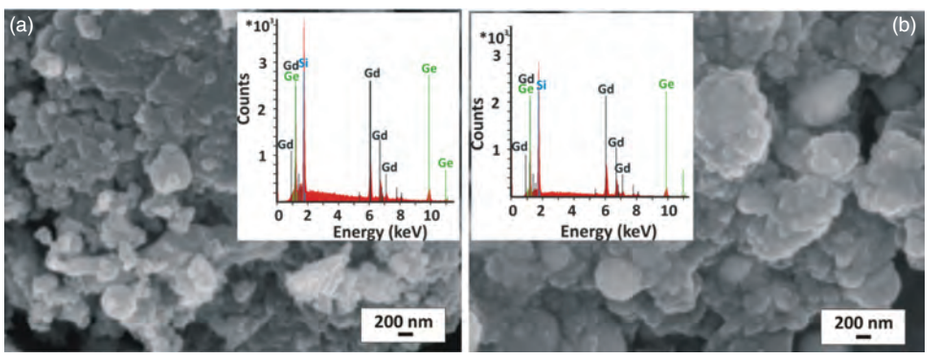

Figure 3. SEM images of powders produced by sequential laser ablation of Si, Gd and Ge targets in ethanol: (a) as-fabricated and (b) after additional laser irradiation.

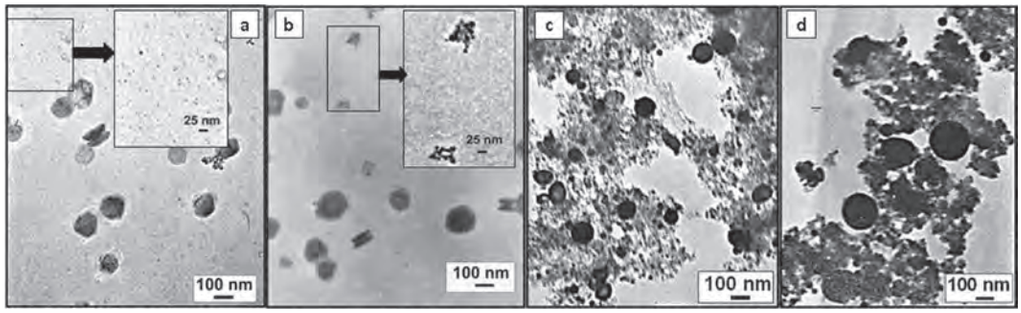

Figure 4. TEM images of NPs prepared by laser ablation in ethanol: (a) after laser ablation of silicon, (b) after laser ablation of Gd in Si colloidal solution, (c) after ablation of Ge in the Si–Gd colloidal solution, (d) after additional laser modification of the colloidal solution prepared on the third step.

phase has a room temperature monoclinic $Gd_5Si_2Ge_2$-type crystal structure when $0.5 \leq x \leq 0.76$. Finally, the Ge-rich Sm_5Ge_4-type solid solution belongs to the so-called orthorhombic II crystal structure when $0.8 \leq x \leq 1$. In the region $0.76 < x < 0.8$ a narrow two-phase region exists.[43]

Since three crystal structures of the $Gd_5(Si_{1-x}Ge_x)_4$ system are closely related to each other and contain the same building block their powder diffraction patterns are also rather similar.

They contain two distinct groups of overlapped Bragg peaks at 2θ between ~30° and 40°, and ~48° and 58°. Because of the similarities of the X-ray powder diffraction patterns, their complexity and broadening the diffraction peaks with the particle size reduction, the establishment the presence of the $Gd_5(Si_{1-x}Ge_x)_4$ alloys in the synthesized powder can not be achieved by X-ray powder diffraction alone. The measurement of the magnetic properties is important because Curie temperatures of the alloys are critically dependent on the composition, in particular

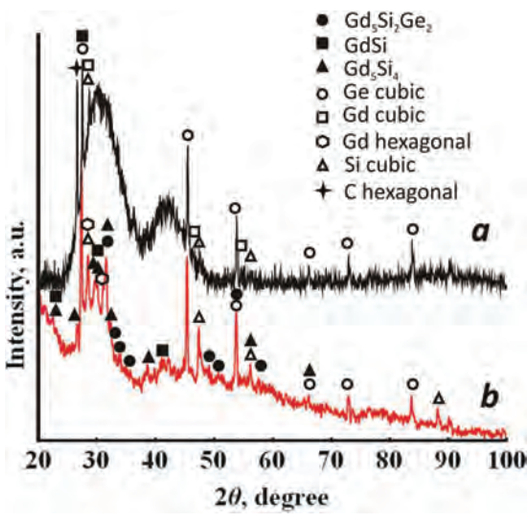

Figure 5. X-ray diffraction patterns of the samples produced by sequential laser ablation of Si, Gd and Ge targets in ethanol as-prepared (a) and after 532 nm laser treatment under laser fluence of 0.23 J/cm^2 (b).

in the monoclinic $Gd_5Si_2Ge_2$-type and the orthorhombic Sm_5Ge_4-type phase regions.

Laser irradiation of colloidal solutions resulted in the changes of the X-ray diffraction diagram. Figure 5(b) represents XRD pattern of the Si–Gd–Ge sample after the additional 532 nm laser irradiation. As can be seen, laser processing of the sample induces significant decreasing of the halo intensity, phase transition from cubic to hexagonal gadolinium, decreasing of cubic germanium peaks and increasing of the germano–silicide peaks intensity. Many of them are separated from the noise as can be seen in the Figure 5(b). These features indicate an improvement of the sample crystallinity. The major peaks of the monoclinic $Gd_5Si_2Ge_2$ and orthorhombic Gd_5Si_4 and GdSi structures are observed more distinctively after laser treatment of the sample. For example, a presence of the monoclinic $Gd_5Si_2Ge_2$ phase is confirmed by the reflections from planes (112), (042), ($2\bar{3}1$), (231), (202), ($1\bar{5}1$) and (080), Gd_5Si_4–(112), (211), (141), (132), (231), (212), (311), (251), (214) and (441), GdSi (space group (Pnma (62))–(200), (201), (111), (210), (112), (020) and (213).[44]

3.2. Properties of NPs Formed by Si–Ge–Gd Sequential Laser Ablation (Sample B)

The extinction spectra of samples of the suspended NPs prepared in ethanol by sequential laser ablation of silicon, germanium and gadolinium targets are similar to the spectra of NPs obtained by sequential laser ablation of these targets in the other sequence: silicon, gadolinium, germanium which was discussed in the previous section. The spectra were rather featureless and exhibited the gradual decrease in overall absorption with increasing wavelength. After laser irradiation the colloids became more transparent in the visible spectral region.

The TEM images of the prepared NPs are shown in Figure 6. The micrograph in Figure 6(a) reveals that after laser ablation (1064 nm) of Si target in ethanol small spherical particles with the mean diameter of about 5 nm and with narrow size distribution are formed. Laser ablation of Ge in Si colloidal solution prepared on the first step results in the formation of a mixture of two types

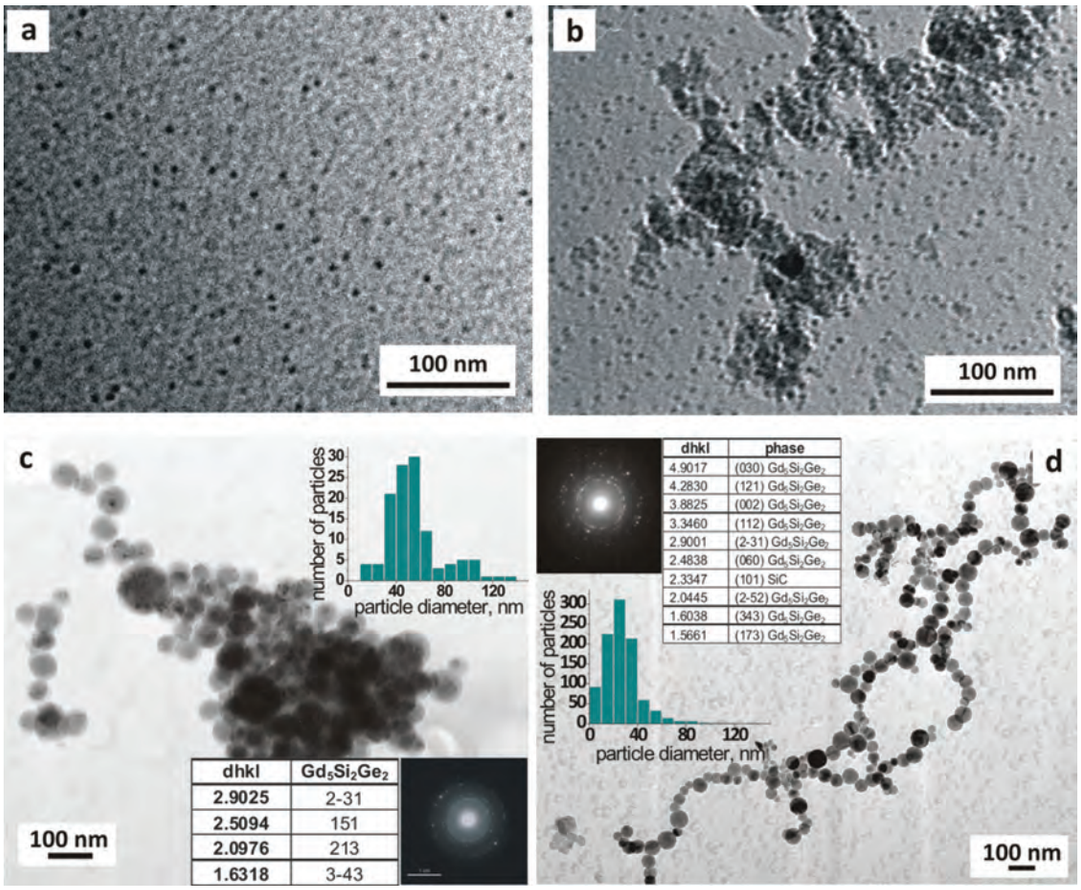

Figure 6. TEM images of NPs prepared by laser ablation in ethanol: (a) after laser ablation of silicon, (b) after laser ablation of Ge in Si colloidal solution, (c) after ablation of Gd in the Si–Ge colloidal solution, (d) after additional laser modification of the colloidal solution prepared on the third step.

of particles that are easily distinguishable in Figure 6(b): small particles and larger agglomerated ones. At the third stage of the process after ablation of Gd in the Si–Ge colloidal solution a consolidation of small particles into the bigger ones with a mean size of 50 nm is observed. TEM micrograph presented in Figure 6(c) reveals loosely aggregated clusters containing single spherical particles. Additional laser irradiation results in the disappearing of the large aggregates and decreasing in diameter of the formed NPs from 50 to 20 nm as can be concluded from the inset in Figure 6(d). Besides, size distribution is significantly narrowing.

Since it was difficult to determine the phase composition of the powder prepared after sequential Si–Ge–Gd laser ablation from their XRD patterns, a crystalline structure of the prepared NPs was found by SAED. The ring patterns were analyzed using a standard computer program, and the lattice interplanar spacings corresponding to the rings were obtained. To check the phases obtained, the interplanar distances were compared with their bulk counterpart data from the literature or from the JCPDS files.[44]

The insets in Figures 6(c) and (d) are the respective selected-area electron-diffraction patterns of the Si–Ge–Gd samples before and after laser treatment. They show well-defined rings characteristic to the randomly oriented nanocrystals. Indexing of the diffraction pattern in Figure 6(c) suggests that the rings corresponded well to the $(2\bar{3}1)$, (142), (213) and $(2\bar{3}4)$ planes of monoclinic $Gd_5Si_2Ge_2$ (space group P21/a (14)), as can be seen from the table in Figure 6(c). From these interplanar distances, the lattice parameters were determined: $a = 7.73$, $b = 15.12$, $c = 7.64$, $\gamma = 87.21°$ that are close to the values provided in JCPDS file No 87-2730 ($a = 7.5808$, $b = 14.802$, $c = 7.7799$, $\gamma = 93.190°$).[44] Hence, it is possible to make the conclusion, that the lattice is distorted.

It should be noted that EDX spectra indicated the presence of only Gd, Si, Ge and Cu in the area being studied (Cu is from the copper support grid). This result confirms that alloyed germano–silicide NPs can be formed by sequential laser ablation of silicon, germanium and gadolinium targets in ethanol.

The phase composition of NPs (and its possible changes) after additional laser irradiation with the second

harmonic of Nd-YAG laser analyzed from their SAED pattern is shown in the inset of Figure 6(d). The interplanar spacings were measured as above, and again corresponded to (030), (121), (002), (112), (2$\bar{3}$1), (060), (2$\bar{5}$2), (343) and (173) planes of the monoclinic $Gd_5Si_2Ge_2$. However trace amount of the cubic silicon carbide phase is also formed after laser treatment. The $Gd_5Si_2Ge_2$ lattice parameters calculated using the diffraction data were found to be: $a = 7.67$, $b = 14.93$, $c = 7.74$, $\gamma = 86.42°$, that is closer to the stoichiometric values than in the case of the non-irradiated sample. It proves that additional laser irradiation of the colloidal solutions results in the improvement of crystallinity of the prepared NPs.

In contrast to the X-ray diffraction patterns with an excess of Ge, the electron diffractograms indicate no evidence of pure Ge. Therefore this phase most probably corresponds to the unreacted sedimented microparticles presented in the powder used for XRD analysis.

3.3. Preparation of NPs by Laser Treatment of Thermally Alloyed Si, Ge, Gd Powders (Sample C)

XRD pattern of the sample produced by thermal processing of the mixture of Gd, Si, Ge micro-sized powders in argon atmosphere confirmed the formation of the $Gd_5Si_2Ge_2$ alloy in one-step process. Figure 7 shows the XRD patterns of the prepared sample. From qualitative analysis according to the standard powder diffraction file (PDF)[44] it is clear that proper heat treatment procedure resulted in the formation of monoclinic $Gd_5Si_2Ge_2$-type structure with a small admixture of the cubic silicon carbide and germanium oxide.

The calculated from the diffraction pattern $Gd_5Si_2Ge_2$ lattice parameters were: $a = 7.481$, $b = 14.962$, $c = 7.8$, $\gamma = 85.1065°$, that are close to the values reported in the literature.

It should be noted that diffraction peaks which could be attributed to unreacted phases of Gd, Si and Ge were not found in the XRD patterns. The absence of the virgin components in the product after thermal heating of their mixture was also confirmed by Raman analysis

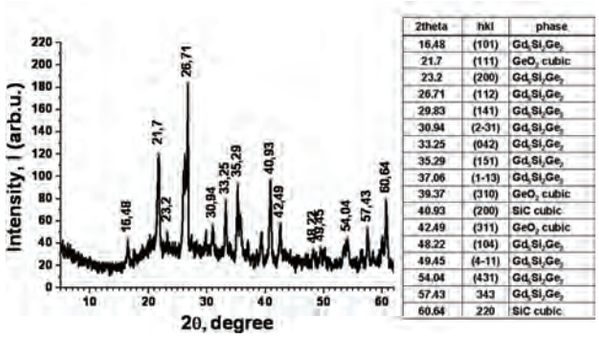

2theta	hkl	phase
16.48	(101)	$Gd_5Si_2Ge_2$
21.7	(111)	GeO_2 cubic
23.2	(200)	$Gd_5Si_2Ge_2$
26.71	(112)	$Gd_5Si_2Ge_2$
29.83	(141)	$Gd_5Si_2Ge_2$
30.94	(2-31)	$Gd_5Si_2Ge_2$
33.25	(042)	$Gd_5Si_2Ge_2$
35.29	(151)	$Gd_5Si_2Ge_2$
37.06	(1-13)	$Gd_5Si_2Ge_2$
39.37	(310)	GeO_2 cubic
40.93	(200)	SiC cubic
42.49	(311)	GeO_2 cubic
48.22	(104)	$Gd_5Si_2Ge_2$
49.45	(4-11)	$Gd_5Si_2Ge_2$
54.04	(431)	$Gd_5Si_2Ge_2$
57.43	343	$Gd_5Si_2Ge_2$
60.64	220	SiC cubic

Figure 7. XRD pattern of the $Gd_5Si_2Ge_2$ alloy prepared by thermal treatment of a mixture of Gd, Si, Ge micropowders.

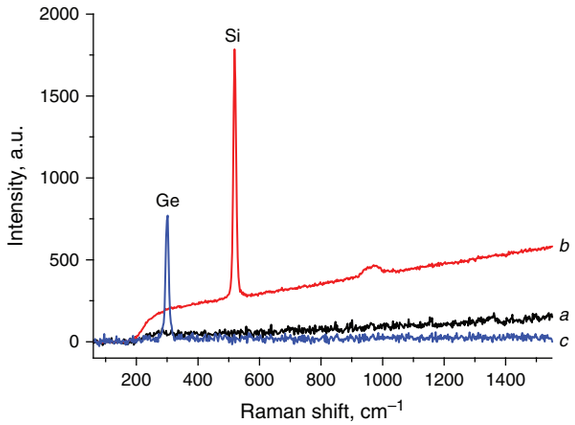

Figure 8. Raman spectra of a sample prepared by thermal treatment of the mixture of Gd, Si, Ge micropowders (a), as well as of silicon (b) and Ge (c) starting materials.

(Fig. 8). No peaks characteristic to germanium and silicon is observed in the resultant powder (graph a), which proves that the powder formed is not a mixture of Gd, Si and Ge powders.

Laser irradiation of the suspension prepared from the synthesized composite causes fragmentation of the initial particles and formation the spherical NPs with a mean diameter of 25 nm. TEM image of NPs formed after 532 nm laser irradiation of Gd–Si–Ge alloy suspension is shown in Figure 9. It is assumed that the primary mechanism for reducing the particle size is a laser-induced fragmentation of the particles in result of the absorption of laser radiation.

The magnetic properties of the synthesized Gd-germano–silicides powders were investigated in the temperature range $7 < T < 1000$ K and in external fields up to 14 T. The results are summarized in Figures 10 and 11.

The magnetization curve, recorded for the obtained powder at low temperatures (7 K) is presented in Figure 10. It can be seen a small magnetic hysteresis

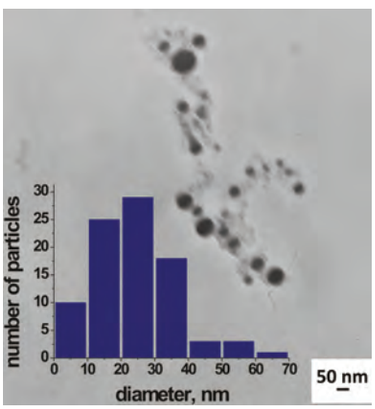

Figure 9. TEM image of NPs formed after 532 nm laser irradiation of Gd–Si–Ge alloy suspension with a size distribution of NPs in the inset.

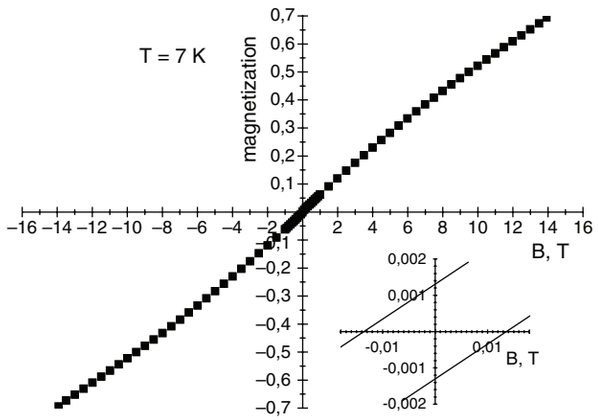

Figure 10. Magnetization of the $Gd_5Si_2Ge_2$ nanopowder plotted as a function of the magnetic field.

effect. The analogical magnetization curves were obtained for temperatures of 77 K and 300 K which could be characterized by a tendency of magnetization values decreasing and narrowing of the magnetic hysteresis loops towards higher temperatures.

As can be seen from Figure 10 the magnetization at 7 K does not reach saturation by varying the magnetic field up to 15 T. The sample prepared exhibits the ferromagnetic behavior with a small hysteresis loop.

It should be noted that the value of the specific magnetization in the 10 T magnetic field was found to be 36.8 A m^2/kg that yields a value of the effective magnetic moment of approximately 6.1 μB which is less than the theoretical value of 7.94 μB per Gd^{3+} ion (μB is the Bohr magneton).

The Curie temperature, T_C, of the synthesized powder was determined from the performed magnetization versus temperature measurements. A typical result of these measurements (thermomagnetic curve) is displayed in Figure 11 where the temperature dependence of magnetization for continuous heating and cooling in 0.1 T magnetic field is shown.

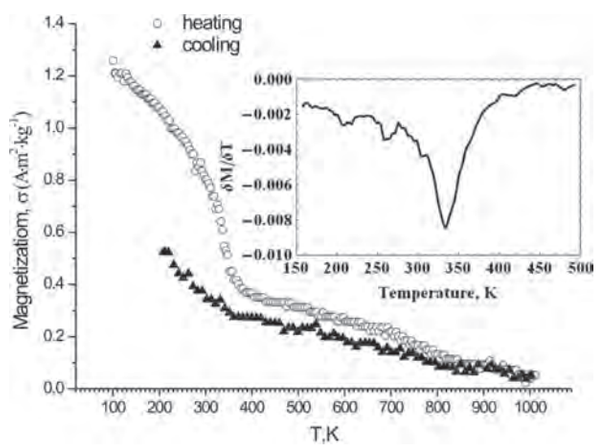

Figure 11. Thermo-magnetic curve of the $Gd_5Si_2Ge_2$ powder, the inset shows the derivative of the magnetization ($\delta M/\delta T$) versus T data.

As can be seen from Figure 11 the thermo-magnetic curve of the synthesized powder displays two transitions: a transition around 260 K and a broad transition around 320 K (from 280 to 360 K). These transitions can be clearly seen in the inset of Figure 11, which shows the derivative of the magnetization ($\delta M/\delta T$) versus T data. For comparison, the bulk $Gd_5Si_2Ge_2$ alloy has two ferromagnetic transitions: one, a first-order coupled magneto structural transition from orthorhombic (ferromagnetic-I) to monoclinic (ferromagnetic-II) at 269 K and the other, a second-order magnetic transition from ferromagnetic (I) to paramagnetic at 299 K.[45–48]

The values of the Curie temperatures are very sensitive to the Si-to-Ge ratio. It is known that Gd_5Si_4 orders ferromagnetically at 335 K while Gd_5Ge_4 orders antiferromagnetically at much lower temperature.[47,48] Substitution of Si by Ge atoms in $Gd_5Si_2Ge_2$ structure results in the decrease of Curie temperature from 335 to 295 K.[49]

The broad magnetic transition behavior observed in the Gd–Si–Ge nanopowder unlike the bulk, can be attributed to particle size reduction, particle size distribution, strain/defects that have an effect on magnetic properties of the sample.

4. DISCUSSION

In addition to the consideration of the properties of the produced NPs we would like to discuss the possible mechanisms of composite NPs formation during PLAL. In PLAL of a solid target, atoms, ions, and small clusters are formed by many concurrent and interrelated mechanisms such as direct ablation, condensation in the expanding plume, chemical reactions, and nonreactive collisions. One of the mechanisms of formation of NPs by laser ablation in liquid considers the NPs growth in the bubble formed from gaseous ablation products and some amount of the surrounding liquid vaporized.[50,51] Arising after the ablating pulse and expanding steadily, the bubble reaches its maximum size and then collapses. Particle formation is associated with aggregation of the ablated atoms and clusters into small embryonic NPs (seeds) and their growth by assembling the clusters and attachment of free atoms during the plasma cooling. Particle size would be related to the lifetime of the bubble, which is a few hundred microseconds (depending on the sample material and laser fluence). After the bubble collapse the NPs are released in the liquid producing the colloidal solution.

By ablating one sample (Gd or Ge in our case) in colloidal solution of another component (Si in our case) the growth processes are rather similar. If the ablated atoms and seed NPs are chemically inert to the preformed colloidal NPs, they can deposit on the surface of the preformed NPs resulting in a formation of the core–shell structures without migrating the shell atoms into the core

or the mixture of two different NPs. Opposite, when chemical interactions between the ablated (deposited) species and seeds in the colloidal solution can occur, compound NPs could be formed.

We suggest that, most likely, the first scenario takes place during laser ablation of Ge target inside the Si colloidal solution. By ablating the Gd target in Si colloid silicide compounds could be formed. Indeed, from a comparison of Raman spectra of the NPs formed after laser ablating of Gd and Ge plates in silicon colloid could be seen that Si nanocrystalls are present in the sample prepared by ablation of Ge in Si colloid (phase separated mixture is formed) and absent in the product formed after ablation of Gd in the silicon colloidal solution. Analogically, using the third step of laser ablation where the third target was ablated in the colloid prepared after the sequential ablation of the first two elements a generation of either alloy, core–shell structures or phase separated mixture of colloidal NPs could be observed depending upon the order of ablation.

Recently, Yang[52] has showed that four kinds of chemical reactions could take place during PLAL in liquids. These are reactions between the ablated species from the target as well as between the reactant species from the target and from the liquid inside the laser-induced bubble. The third kind of chemical reactions occurs at the plasma–liquid interface, and finally the chemical reactions between the ablated species and the liquid constituents can occur inside the liquid. On the basis of thermodynamic parameters of the plasma plume, he analyzed the basic physical and chemical processes in the nanophase formation during laser ablation in liquids, including nucleation, phase transition, and growth, and concluded that various compounds could be synthesized in the high-temperature and high-pressure environment.[42, 52] From the viewpoint of thermodynamics, the formation of new compounds should occur as a result of collisions between the species in relatively high-energy states, while the nucleation may result from aggregations of the neutral species. It should be noted that in addition to the thermodynamic conditions similar evolution of time–space distributions of reagents is also required for effective chemical interactions between the ablated species.

Because of the experimental difficulties the determination of composition and structure of the matter inside the bubble during its evolution is still a challenge and the stages of PLAL where main chemical processes that define the stoichiometry, phase composition and size distribution of the final products have not been clearly identified. In our case of sequential laser ablation chemical reactions resulting in compound gadolinium germano–silicides formation could occur during the cavitation bubble collapse which may drive chemical reactions and phase transitions[53] and at the bubble/liquid interface containing species of both elements.

And finally, post-ablation laser irradiation can be used as a tool to change not only the particle morphology, but their composition and inner structure through the photoinduced heating, melting and chemical interactions. If the absorbed energy is high enough, the particles can melt, which favours the reaction of the molten NP with the other NPs in the same solution to form nanocomposite particles. Their spherical shape clearly indicates melt formation during the irradiation process suggesting that the temperature of NPs transiently increases above the melting point. The possibility of particle heating with consequent melting and evaporation in our experiments was supported by estimating a temperature of particles, which can be reached in result of the absorption of laser light. The temperature of the particles was estimated on the basis of a balance between the absorbed laser energy and heat losses during the laser pulse using the bulk physical constants. The calculations showed that temperature of the Gd NPs with radius of 10 nm exceeds the melting point of Gd (1585 K) at the laser fluencies used and is 2100 K for 230 mJ/cm^2 and 2600 K for laser fluence of 400 mJ/cm^2. Thus, the calculated heat required to melt the particles roughly agreed with the value of the experimental threshold of laser fluence for particle modification.[54]

5. CONCLUSIONS

Laser assisted techniques in liquid based on laser ablation from an alloy pellet and sequential ablation from elemental targets with subsequent laser post-ablation treatment to alloy the formed clusters have been demonstrated to be a tool to prepare magnetic gadolinium germano–silicides particles with sizes in the nanometric range. In fact, three types of samples were prepared: Sample A by the sequential ablation of the Si–Gd–Ge targets with additional laser irradiation of formed colloids; Sample B by the sequential ablation of the Si–Ge–Gd targets with additional laser irradiation and Sample C by laser re-dispersing of the thermally alloyed Gd–Si–Ge microparticles. For practical applications a good approach to the effective production of Gd–Si–Ge alloys provides two-step process involving thermal alloying of the stoichiometric mixture of Gd, Si and Ge powders with subsequent laser-induced fragmentation of the alloyed microparticles. The synthesized particles (mean diameter 25 nm, major phase monoclinic $Gd_5Si_2Ge_2$) exhibit the magnetic transition at the ordering temperature T_C in the desired range (315–320 K) and can be tested for their potential application in the method of magnetic hyperthermia treatment. Compared to the sample A, sample B produced by sequential laser ablation of Si–Ge–Gd targets was mainly comprised of near-spherical nanoparticles with narrow size distribution, mean diameter of 20 nm and monoclinic $Gd_5Si_2Ge_2$ as a major phase. Therefore, with the thorough selection of the synthesis conditions the employed approach of sequential ablation also offers interesting possibilities towards production of

complex nanomaterials and warrants further research. It is expected, that the obtained results will serve a basis for further studies of heating characteristics and optimization of preparation conditions to meet the optimal temperature required in self-controlled magnetic fluid hyperthermia.

Acknowledgments: This work has been supported by the National Academy of Sciences of Belarus under project Convergence 2.6.04 and the Belarusian Foundation for Fundamental Researches under Grant No. F 14SRB-008. The authors would like to thank Dr. K. I. Yanushkevich for the magnetic and XRD measurements and fruitful discussions.

References and Notes

1. G. W. Yang, Laser Ablation in Liquids: Principles and Applications in the Preparation of Nanomaterials, Pan Stanford Publishing, Singapore **(2012)**.
2. V. Amendola and M. Meneghetti, *Phys. Chem. Chem. Phys.* 15, 3027 **(2013)**.
3. S. Barcikowski and G. Compagnini, *Phys. Chem. Chem. Phys.* 15, 3022 **(2013)**.
4. N. V. Tarasenko and A. V. Butsen, *Quantum Electron.* 40, 986 **(2010)**.
5. G. Compagnini, A. A. Scalisi, and O. Puglisi, *J. Appl. Phys.* 94, 7874 **(2003)**.
6. H. Zeng, X.-W. Du, S. C. Singh, S. A. Kulinich, S. Yang, J. He, and W. Cai, *Adv. Funct. Mater.* 22, 1333 **(2012)**.
7. P. Liu, Y. Liang, X. Z. Lin, C. X. Wang, and G. W. Yang, *ACS Nano* 5, 4748 **(2011)**.
8. C. C. Berry, *J. Phys. D: Appl. Phys.* 42, 224003.1 **(2009)**.
9. A. Hahn and S. Barcikowski, *JLMN-J. Laser Micro/Nanoeng.* 4, 51 **(2009)**.
10. S. Petersen and S. Barcikowski, *Adv. Funct. Mater.* 19, 1167 **(2009)**.
11. J. P. Sylvestre, S. Poulin, A. V. Kabashin, E. Sacher, M. Meunier, and J. H. T. Luong, *J. Phys. Chem. B* 108, 16864 **(2004)**.
12. N. V. Tarasenko, A. V. Butsen, M. I. Nedelko, and N. N. Tarasenka, *J. Phys. Chem. C* 116, 3897 **(2012)**.
13. N. N. Tarasenka, A. V. Butsen, V. V. Pankov, and N. V. Tarasenko, *Phys. Status Solidi B* 250, 809 **(2013)**.
14. C. S. S. R. Kumar and F. Mohammad, *Adv. Drug Delivery Rev.* 63, 789 **(2011)**.
15. S. Fossheim, K. Il'yasov, J. Hennig, and A. Bjørnerud, *Academic Radiol.* 7, 1107 **(2000)**.
16. L. H. Lindner, H. M. Reinl, M. Schlemmer, R. Stahl, and M. Peller, *Int. J. Hyperthermia.* 21, 575 **(2005)**.
17. R. Sharma and C. J. Chen, *J. Nanopart. Res.* 11, 671 **(2009)**.
18. S. N. Ahmad and S. A. Shaheen, *Key Eng. Mater.* 442, 242 **(2010)**.
19. S. N. Ahmad, Y. Akin, and S. A. Shaheen, *J. Appl. Phys.* 97, 10Q902.1 **(2005)**.
20. P. Tartaj, M. D. P. Morales, S. Veintemillas-Verdaguer, T. González-Carreño, and C. J. Serna, *J. Phys. D: Appl. Phys.* 36, R182 **(2003)**.
21. F. L Fajardo, *Cancer Res.* 44, 4826s **(1984)**.
22. E. M. Levin, K. A. Gschneidner, Jr., and V. K. Pecharsky, *J. Magn. Magn. Mater.* 231, 135 **(2001)**.
23. K. H. J. Buschow, Handbook of Magnetic Materials, Elsevier, Amsterdam **(2008)**, Vol. 17.
24. X. Bohigas, E. Molins, A. Roig, J. Tejada, and X. X. Zhang, *IEEE Transactions on Magnetics* 36, 538 **(2000)**.
25. Y. Chen, J. Wu, S. Xiao, T. Zhang, Y. Tang, and M. Tu, *J. Alloys Compd.* 422, 21 **(2006)**.
26. M. Engström, A. Klasson, H. Pedersen, C. Vahlberg, P.-O. Käll, and K. Uvdal, *Magn. Reson. Mater. Phys. Biol. Med.* 19, 180 **(2006)**.
27. G. Liang, J. Ronald, Y. Chen, D. Ye, P. Pandit, M. L. Ma, B. Rutt, and J. Rao, *Angew. Chem. Int. Ed.* 50, 6283 **(2011)**.
28. L. Zhou, Z. Gu, X. Liu, W. Yin, G. Tian, L. Yan, S. Jin, W. Ren, G. Xing, W. Li, et al. *J. Mater. Chem.* 22, 966 **(2012)**.
29. C. Rümenapp, B. Gleich, and A. Haase, *Pharm Res.* 29, 1165 **(2012)**.
30. C.-L. Tseng, I.-L. Shih, L. Stobinski, and F.-H. Lin, *Biomaterials* 31, 5427 **(2010)**.
31. G. Greil, A. Powell, H. Gildein, and T. Geva, *J. Am. Coll. Cardiol.* 39, 335 **(2002)**.
32. G. Chen, H. Qiu, P. N. Prasad, and X. Chen, *Chem. Rev.* 114, 5161 **(2014)**.
33. S. Parveen, R. Misra, and S. K. Sahoo, *Nanomed. Nanotech. Biol. Med.* 8, 147 **(2012)**.
34. D. Stefanakis and D. F. Ghanotakis, *J. Nanopart. Res.* 12, 1285 **(2010)**.
35. Z. Liu, X. Liu, Q. Yuan, K. Dong, L. Jiang, Z. Li, J. Ren, and X. Qu, *J. Mater. Chem.* 22, 14982 **(2012)**.
36. S. N. Ahmad and S. A. Shaheen, *J. Appl. Phys.* 106, 064701 **(2009)**.
37. Y. D. Yao, Y. Y. Chen, S. F. Lee, W. C. Chang, and H. L. Hu, *J. Magn. Magn. Mater.* 239, 249 **(2002)**.
38. V. S. Burakov, N. V. Tarasenko, A. V. Butsen, V. A. Rozantsev, and M. I. Nedel'ko, *Eur. J. Appl. Phys.* 30, 107 **(2005)**.
39. Z. H. Stachurski, *Materials* 4, 1564 **(2011)**.
40. L. C. Pathak, T. B. Singh, S. Das, A. K. Verma, and P. Ramachandrarao, *Mater. Lett.* 57, 380 **(2002)**.
41. Z.-G. Ban and L. L. Shaw, *J. Mater. Sci.* 37, 3397 **(2002)**.
42. S. Yang, W. Cai, H. Zeng, and X. Xu, *J. Mater. Chem.* 19, 7119 **(2009)**.
43. A. O. Pecharsky, K. A. Gschneidner, Jr., V. K. Pecharsky, and C. E. Schindler, *J. of Alloys and Compounds* 338, 126 **(2002)**.
44. International Centre for Diffraction Data, PCPDFWIN, JCPDS, 1998, V. 2.00, 87-2320; 87-2319; 80-0705; 51-0833; 72-2223; 89-2924; 89-5011; 89-5012; 25-0284; 23-0999; 75-0254.
45. D. M. Rajkumar, M. Manivel Raja, R. Gopalan, and V. Chandrasekaran, *J. Magn. Magn. Mater.* 320, 1479 **(2008)**.
46. V. K. Pecharsky and K. A. Gschneidner, Jr., *Appl. Phys. Lett.* 70, 3299 **(1997)**.
47. V. K. Pecharsky and K. A. Gschneidner, Jr., *Phys. Rev. Lett.* 78, 4494 **(1997)**.
48. F. Holtzberg, R. J. Gambino, and T. R. McGuire, *J. Phys. Chem. Solids* 28, 2283 **(1967)**.
49. G. J. Miller, *Chem. Soc. Rev.* 35, 799 **(2006)**.
50. M. Dell'Aglio, R. Gaudiuso, R. ElRashedy, O. D. Pascale, G. Palazzo, and A. D. Giacomo, *Phys. Chem. Chem. Phys.* 15, 20868 **(2013)**.
51. P. Wagener, S. Ibrahimkutty, A. Menzel, A. Plech, and S. Barcikowski, *Phys. Chem. Chem. Phys.* 15, 3068 **(2013)**.
52. G. W. Yang, *Prog. Mater. Sci.* 52, 648 **(2007)**.
53. P. Liu, Y. L. Cao, C. X. Wang, X. Y. Chen, and G. W. Yang, *Nano Letters* 8, 2570 **(2008)**.
54. N. N. Tarasenka, A. V. Butsen, N. V. Tarasenko, and V. V. Pankov, Book of Proceedings of International Conference on Physics, Chemistry and Application of Nanostructures, edited by V. E. Borisenko, World Scientific Publishing, Singapore **(2013)**, p. 385.

Received: 8 July 2015. Accepted: 28 July 2015.